Structural Monitoring and Maintenance, *Vol. 2, No. 3 (2015) 253-267*
DOI: http://dx.doi.org/10.12989/smm.2015.2.3.253

Monitoring corrosion of reinforced concrete beams in a chloride containing environment under different loading levels

Aifang Wei[a], Ying Wang[b] and Mike Y.J. Tan[*]

School of Engineering, Deakin University, 75 Pigdons Rd, Waurn Ponds, Victoria 3216, Australia

(Received March 9, 2015, Revised August 11, 2015, Accepted August 23, 2015)

Abstract. Corrosion has significant adverse effects on the durability of reinforced concrete (RC) structures, especially those exposed to a marine environment and subjected to mechanical stress, such as bridges, jetties, piers and wharfs. Previous studies have been carried out to investigate the corrosion behaviour of steel rebar in various concrete structures, however, few studies have focused on the corrosion monitoring of RC structures that are subjected to both mechanical stress and environmental effects. This paper presents an exploratory study on the development of corrosion monitoring and detection techniques for RC structures under the combined effects of external loadings and corrosive media. Four RC beams were tested in 3% NaCl solutions under different levels of point loads. Corrosion processes occurring on steel bars under different loads and under alternative wetting - drying cycle conditions were monitored. Electrochemical and microscopic methods were utilised to measure corrosion potentials of steel bars; to monitor galvanic currents flowing between different steel bars in each beam; and to observe corrosion patterns, respectively. The results indicated that steel corrosion in RC beams was affected by local stress. The point load caused the increase of galvanic currents, corrosion rates and corrosion areas. Pitting corrosion was found to be the main form of corrosion on the surface of the steel bars for most of the beams, probably due to the local concentration of chloride ions. In addition, visual observation of the samples confirmed that the localities of corrosion were related to the locations of steel bars in beams. It was also demonstrated that electrochemical devices are useful for the detection of RC beam corrosion.

Keywords: corrosion; reinforced concrete beams; electrochemical devices; loading; galvanic current

1. Introduction

Reinforced concrete (RC) plays a very important role in the construction industry worldwide, because of its versatility, low price, and especially its advantage of being resilient to extreme environmental conditions (Lomborg 2001). The effective bonding between a steel bar and concrete can take advantage of physical, mechanical and chemical properties for both materials. Unfortunately, adverse effects from factors such as corrosion may decrease the bonding force, and lead RC structural elements to durability reduction, serviceability decrease, bond strength drop and longitudinal cracking (Cabrera 1996). Corrosion of rebar in concrete is generally recognised as one

*Corresponding author, Professor, E-mail: mike.tan@deakin.edu.au
[a] E-mail: amyaifang@gmail.com
[b] Ph.D., E-mail: ying.wang@deakin.edu.au

Copyright © 2014 Techno-Press, Ltd.
http://www.techno-press.org/?journal=smm&subpage=7 ISSN: 2288-6605 (Print), 2288-6613 (Online)

of the major failure mechanisms of RC structures. Therefore, enormous resources have been spent on the maintenance and retrofitting of civil infrastructure all over the world in order to control corrosion. It is estimated that the annual cost for corrosion management exceeded $1.8 trillion worldwide (Schmitt 2009) and that the total annual cost of corrosion in the US exceeded $1 trillion in 2013 (Nwaubani and Katsanos 2014). The corrosion process in the civil infrastructure is inevitable because steel rebar corrosion in marine environments is thermodynamically spontaneous, however corrosion monitoring/detection techniques could help to minimize the corrosion damage and costs. Firstly, corrosion monitoring could help predicting, identifying and managing factors influencing corrosion. This could prevent unexpected failure of RC structures due to corrosion. Secondly, corrosion monitoring enables asset owners to prioritise site survey and inspection operations, and to develop rehabilitation measures and maintenance strategies for maintaining and managing RC structures. Thirdly, information from corrosion monitoring tools can help generating a lifetime reliability model for RC structures. These models could help predicting and extending the safe operational life of major infrastructures.

It is known that the corrosion processes of RC structures are affected by factors such as the presence of chlorides, changes in temperature/moisture levels, the duration of environmental exposure, and mechanical loadings (Díaz *et al*. 2009). For instance chloride ion concentration in concrete is known to be one of the major factors affecting steel rebar corrosion, especially in marine environment (Fang *et al.* 2006). In marine structures, chloride ions can enter concrete through processes facilitated either by water penetrated from the outside (Ormellese *et al*. 2006), or by carbonation in RC (Dehwah 2002). Chloride is believed to induce steel bar corrosion by damaging protective oxide layers at the interface of steel and concrete covers (Poupard et al. 2006), leading to the development of active localized corrosion macrocells (Assouli *et al*. 2008). A wetting-drying cycle has also been identified as a factor affecting the corrosion of RC structures (Sakr 2005) in natural marine environment that has been simulated in the laboratory (Yuan et al., 2007) and has been found to cause accelerated corrosion on the surface of steel bars (Torres-Acosta *et al.* 2007). This increased corrosion has been explained by the increase of corrosion potential differences between the anode and cathode areas on the steel rebar and the decrease of concrete resistance in wetting - drying cycle conditions (Li *et al.* 2005). Another factor affecting the corrosion of RC structures is the duration of environment exposure. The reductions in the mechanical strength of steel bars could happen when the steel bars are exposed in the corrosion environment (Apostolopoulos and Papadakis 2008). The corrosion propagation period can last up to 50 years, depending upon the performance of electric resistivity and the oxygen availability of the concrete (Pettersson 1998). Furthermore, mechanical loadings were found to affect chloride transport in concrete and lead to higher corrosion rates of the steel rebar and early cracks on the surface of RC structures (Wang *et al.* 2011).

Various techniques have been applied to determine the rates and patterns of corrosion in RC structures. One of the most popular techniques is electrochemical measurement that allows the determination of corrosion related parameters such as half-cell potential, concrete resistivity, and corrosion current density (Ahmad 2003). The half-cell potential measurement is a technique of determining corrosion tendency by measuring corrosion potential using a reference electrode and a voltmeter. Half-cell potential measurement was used for establishing a corrosion initiation indicator in a concrete structure by Pradhan and Bhattacharjee (2009). Due to its measurement simplicity and cost effectiveness, the corrosion potential measurement method has been widely used in testing the corrosion of steel bars in RC structures (Assouli *et al*. 2008). On the other hand, the measurement of concrete electrical resistivity is also applied to evaluate the corrosion level at

any special location in RC structures because the concrete resistivity significantly affects the electrochemical corrosion currents flowing in a concrete structure (Berkeley and Pathmanaban 1990). The corrosion current density measurement has been suggested as a useful quantitative parameter in quantifying the corrosion of RC. The method of measuring electrochemical Linear Polarization Resistance (LPR) using a potentiostat has been employed to measure corrosion current density. A gravimetric weight loss method was utilised to estimate the correlation between measured corrosion rate and reinforcement weight loss (Alghamdi and Ahmad 2014). However, it should be noted that there are a number of difficulties in applying the LPR method to on-site corrosion measurement of RC structures due to factors such as the high resistance between concrete and steel bars (Ahmad 2003). Conventional electrochemical polarisation based methods can be very difficult to be applied in highly electrically resistive environments where significant corrosion rate measurement errors are often caused by a huge potential drop commonly referred to as IR drop. More importantly, these conventional electrochemical methods can only be used for estimating general corrosion because in principle they are based on the most fundamental relationship in electrochemical kinetics, i.e., Butler-Volmer equation, which only describes the kinetics of uniform corrosion mechanism, and thus does not apply to localised corrosion (Tan 2011). Except for the electrochemical measurement techniques, other monitoring techniques are also applied to corrosion research. For instance Wang *et al*. (2008) carried out the vibration tests in studying its effect on the natural frequency of RC beams fortnightly, and an empirical model was developed from the results to study the relationship between crack width and corrosion loss. Wang and Hao (2012) used both structural vibration and guided wave propagation data to identify structural damage.

Although previous studies have made significant contributions in understanding the effects of various influencing factors on the corrosion of RC structure, few studies have focused on the understanding of the effects of mechanical loading (Apostolopoulos and Papadakis 2008, Ballim and Reid 2003, Song *et al*. 2010). This present work is a preliminary study aiming to understand the corrosion behaviour of RC structures under the combined effects of mechanical stress and corrosive environment. This study focuses on the development of corrosion monitoring and detection techniques, i.e., corrosion galvanic current measurements, for monitoring corrosion processes occurring on steel bars under different loads and alternative wetting - drying cycle conditions.

2. Experimental program

2.1 Specimen design

Four RC beams were fabricated as test specimens in this study. The beams were designed with concrete strength of N30 according to the minimum value required by the standard of AS3600-2009. The concrete mix was designed with the compressive strength of 32 MPa. The proportions of cement, fine sand and coarse aggregate contents were 400 kg/m^3, 650 kg/m^3 and 1138 kg/m^3, respectively. The maximum aggregate size was 14 mm. The w/c ratio was 0.45 and a slump test had been carried out before the concrete was casted. The result of the collapse test was 40 mm, which is in compliance with the standard of AS3600-2009. The dimensions of the beams were 500 mm (length) x 150 mm (height) x 150 mm (width). The concrete cover of the RC beam was 20 mm.

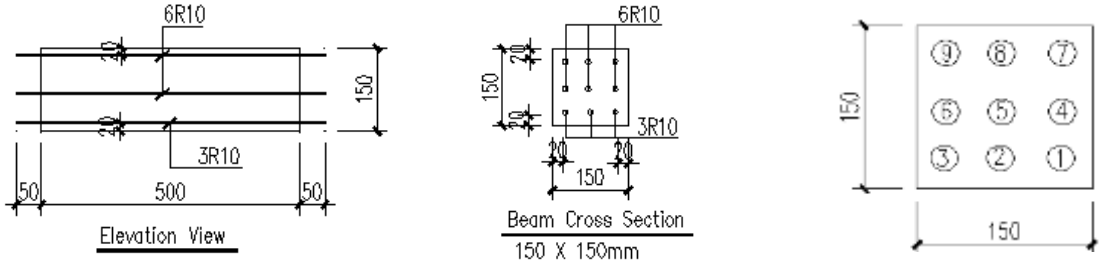

(a) Elevation view (b) Beam cross section (c) Serial numbers for steel bars

Fig. 1 A schematic diagram illustrating concrete beams used in this study

Each RC beam includes 9 steel bars with the nominal diameter of 10 mm (Ø 10). The whole length of each steel bar is 600 mm with 500 mm buried in the concrete and 50mm extending outside of the concrete beam on both sides. This extension was for the convenience of connecting wires in the subsequent corrosion tests. The property of steel bars was D250N, and the steel yield strength was f_{sy}= 250 MPa. All the steel bars had been rubbed with a wire brush to completely remove any rust on the surface before casting. Stirrups were removed in order to leave each rebar being separated. Casting of beams was performed and finished on the same day. Concrete beams were de-moulded after 24 hours of casting and were then cured under water in a bath environment for 28 days in the laboratory. Fig. 1 illustrates elevation view and cross section for the beams, and the serial numbers for steel bars.

Fig. 2(a) shows a concrete beam that was completed casting and curing. In order to investigate the corrosion of steel bars in concrete beams, the exposed sections of bars must be protected from contacting the solution. Therefore, a seven-step procedure was applied, before exposing beams in the 3% NaCl solution for corrosion testing. The first step was to completely clean the rust of steel bars outside of the beams, as the steel bars had been exposed curing in the atmosphere for 28 days. The second step was to connect wires with steel bars separately. The third step was to securely connect the wire and the steel bar using insulating tapes. In the fourth step, a coating of silicone sealant was applied to cover the insulating tapes. The fifth step was to paint steel bars using the bituminous paint, after 24 hours of painting the silicone sealant. In the sixth step, after 24 hours of applying the bituminous paint, the silicone sealant was used again to seal the end of the steel bars. The aim was to protect the bituminous cover from falling out when the wires were taken out of the tank to test. The last step was to mark each wire from 1 to 9 using labels for identification. Fig. 2 (b) shows the protections of specimen and the exposed sections of the bars.

2.2 Experimental setup

A loading rig was developed for this study to allow a sustained load on the concrete beam. A plastic bag covered with petroleum jelly was used to protect the load cells from corrosion attack. In order to protect the concrete beam from stress concentration, a stainless steel plate was placed on the top of the test beam. A stainless steel and watertight tank, which was 300 (width) x 300 (depth) x 800 mm (length), was used to contain 3% NaCl solution and test specimens, as shown in Fig. 3. High purity Milli-Q water was used for mixing the chloride solution. A conductivity meter

was used to check the solution conductivity which had a steady reading of 48.1 mS/cm. All wires were fixed on both side of the tank for the convenience of the potential and galvanic current measurements. Each beam was supported by two Nylon support blocks of 150 mm (length) x 40 mm (width) x 25 mm (height) under the ends of the beam.

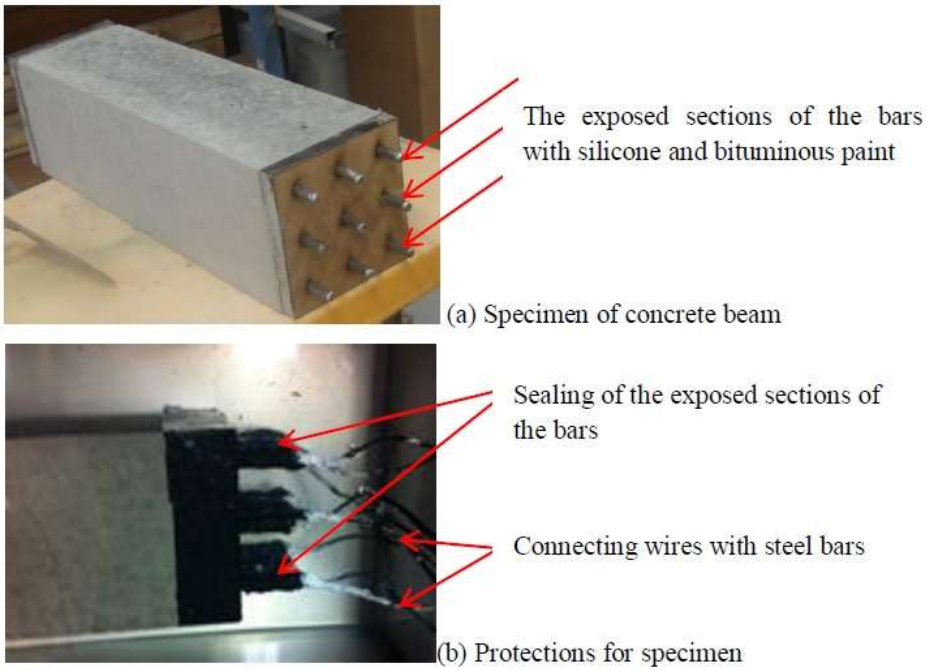

Fig. 2 Specimen for corrosion test

Fig. 3 Experimental setup

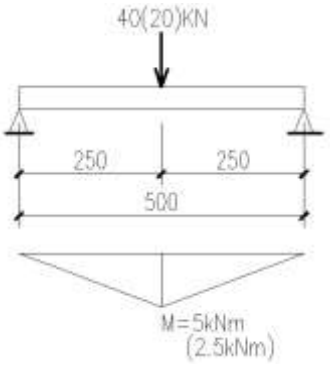

Fig. 4 Force and bending moment diagrams

Different stress levels lead to different force and bending moment in RC structures. Based on the theoretical calculation according to AS3600 - 2009, the ultimate capacity of test specimens is 40.07 kN. To investigate the corrosion rates of the test specimens under different stress levels while not to break the beam, three beams were tested under point loads of 40 kN, 20 kN and 20 kN respectively. Fig. 4 illustrates the force and bending moment diagrams for the tested beams. The test programs of four beams were designed as following:

- Beam 1 was tested under 40 kN in the chloride solution for 2 weeks;
- Beam 2 was tested under 20 kN in the chloride solution for 2 weeks;
- Beam 3 was tested under alternative wetting and drying cycles:
  a. Wetting by submersion in chloride solution while under a 20 kN load for 1 week;
  b. Drying in an indoor environment without loads for 2 weeks;
  c. Finally wetting with loading of 20 kN for one week.
- Beam 4 was tested in the chloride solution without loading for 8 weeks.

2.3 Test equipment and procedure

A Velleman DVM850BL multimeter as well as a reference electrode (Ag/AgCl) were used to measure potential of each steel bar and galvanic currents flowing between bars during the experiment, which was designed in accordance with International Electrotechnical Commission standard IEC-1010. Before the measurements, the concrete surface was prepared by brushing and polishing with abrasive paper. Moreover, the black (negative) test lead was inserted into “COM” jack of this multimeter, and the red test lead (positive) was inserted into the "VΩmA" jack of this multimeter. When testing the galvanic current, the black lead was connected with one selected the steel bars (e.g., the No.1 bar), the red test lead was connected with each of the other 8 steel bars, in sequence, as shown in Fig. 5(a). As a result, the measurement results of galvanic currents, including between No. 1 and No. 2, No. 1 and No. 3, ..., No. 1 and No. 9, were obtained daily over the test period. Since the current was unstable, its final value was the average of electric current values measured in the first 2 minutes. When testing potential results, the black test lead was connected with the reference electrode located on the surface of the concrete beam, and the red test lead was connected with each steel bar, as shown in Fig. 5(b). When all measurements have been completed, each concrete beam was cut into nine parts by a cutting machine. Then, each part was

broken again, so that the steel bars were taken out and cleaned for further investigation. The visual observation was conducted. Finally Scanning Electron Microscope (SEM) images were taken from corroded mild steel bar surface after the samples had been cleaned by HCl solutions.

3. Results and discussion

Fig. 6 shows galvanic current measurement results from four beams. Although the corrosion currents were unstable during the test period, probably due to unstable chloride ion movement in the RC beams (Al Zubaidy and Al Tamimi, 2012), a clear trend can be found that smaller galvanic currents were detected from all steel bars in Beam No. 4 that was not under loading, as shown in Fig. 6 (d). Since the galvanic currents were driven by potential differences between steel bars in each beam, smaller galvanic current values would indicate less corrosion activities. The galvanic current variations between steel bars are also small in Fig. 6(d). The difference between the most positive and negative currents is less than 0.2 mA in Fig. 6(d), while such differences are approximately 0.7 mA in Fig. 6(c), over 1.0 mA in Fig. 6(b) and 0.75 mA in Fig. 6(a). These results probably also suggest less corrosion activity occurred on steel bars in Beam No. 4 that was not under loading. Furthermore, from the absolute values of all current values shown in Fig. 6(b), the top and bottom bars recorded bigger current values than the middle bars. This is probably because the bottom bars were under the effect of higher tensile stress and the top bars have the higher compressive stress, compared to the middle bars that were under much smaller stress (Poerner 2007). The behaviour of Beam 3 in Fig. 6(c) appears to be similar to that of Beam 2 in Fig. 6(b).

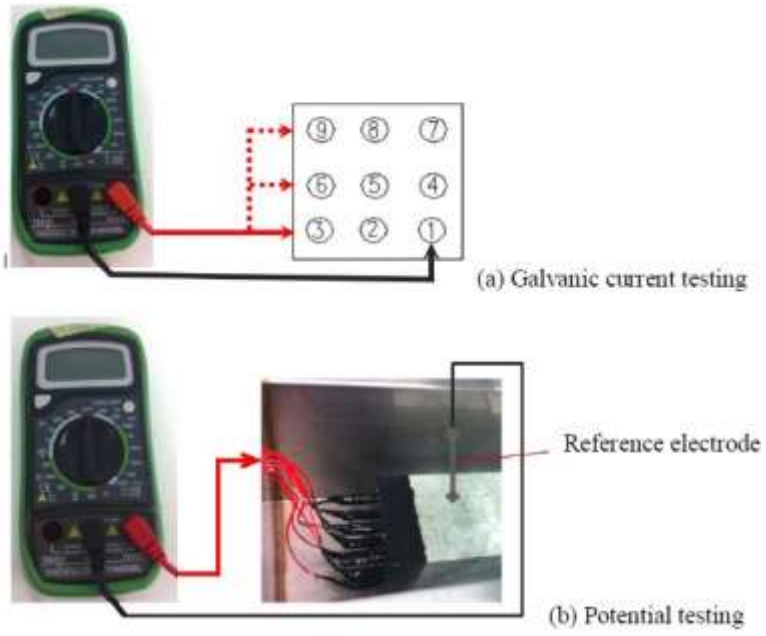

Fig. 5 Velleman DVM850BL Multimeter connections with wires

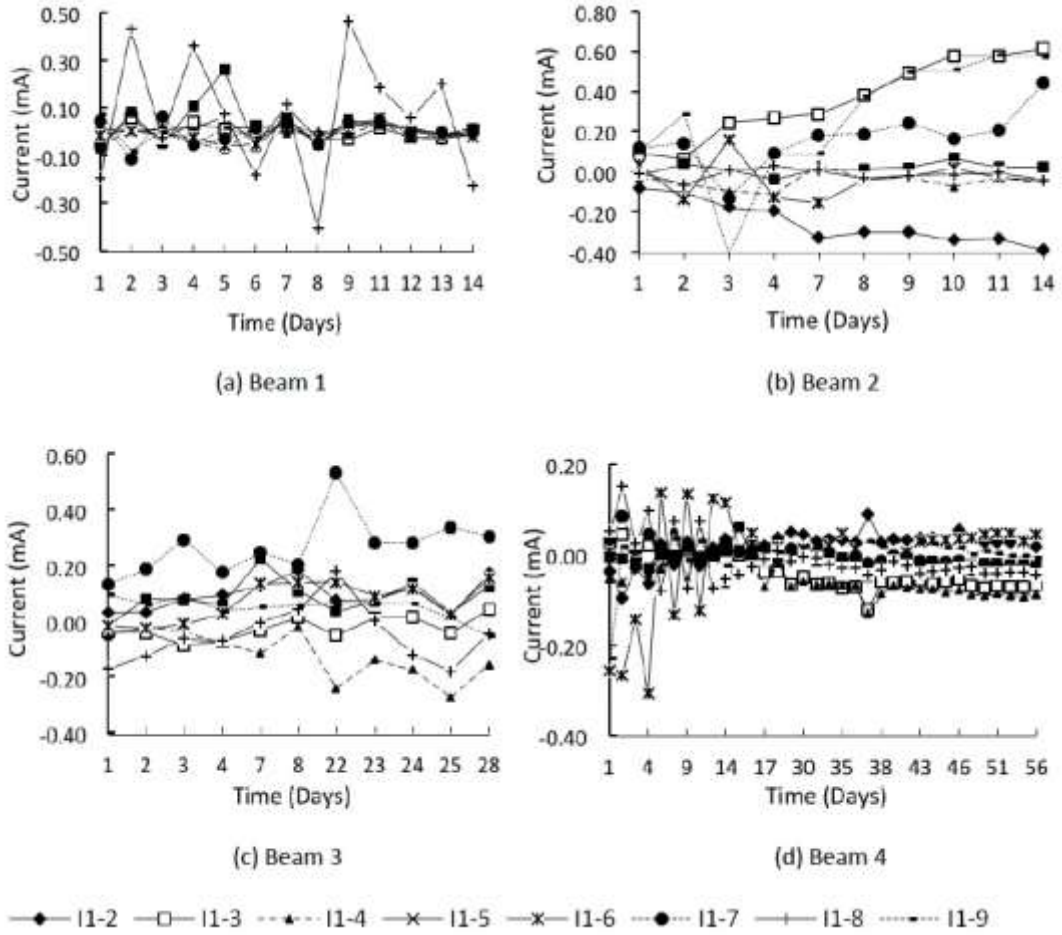

Note: I1-2, I1-3…, and I1-9 represents the current value of steel bars between No.1and No. 2, No. 1 and No. 3, …, No.1 and No. 9 respectively

Fig. 6 Plots of galvanic current values measured from Beam 1, 2, 3, 4

Fig. 7 shows the potential measurement results of four beams. Although a small decreasing trend is observable in some of the figures, such as Fig. 7(a) and Fig. 7(d), major fluctuation is clear in these data. A possible reason is that the potential values are thermodynamic information, which may not correlate with corrosion rates that are a type of kinetics information. Therefore, the results from potential testing are less relevant to corrosion processes in the test beams and are less useful for corrosion monitoring of RC beams than those from the galvanic current testing. To provide further details on the effects of local electrochemical corrosion activities, an appendix has been added to show experimental results (numerical potential and current values) measured from rebar located at different areas of the test beams.

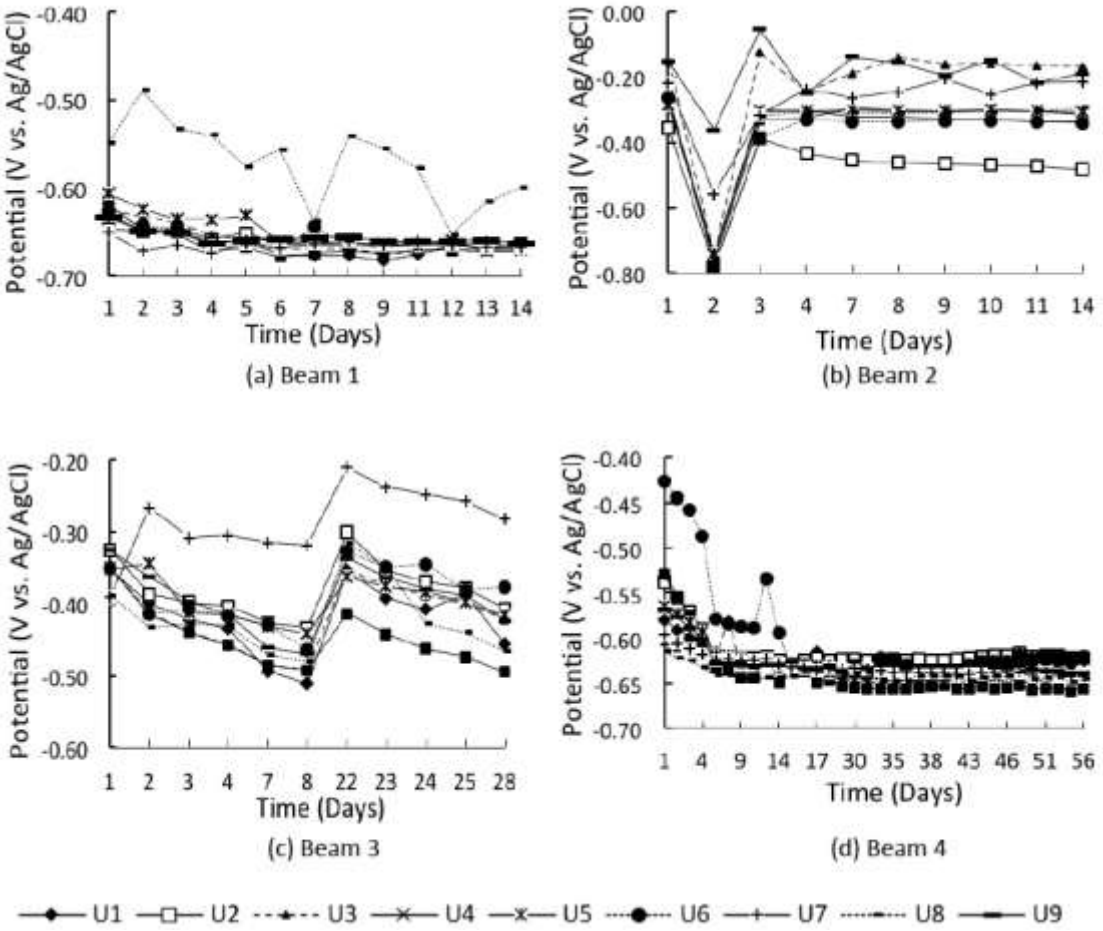

Note: U1, U2, …, and U9 represents potential values for steel bars of No.1, No.2, …, and No.9 respectively

Fig. 7 Plots of potential values measured from Beam 1, 2, 3, 4

Visual observation of the steel bars was carried out after splitting and breaking the beams. As shown in Fig. 8, in general, one or a few pits were observed within a small area on the surface of some of the steel bars. The appearance of corrosion suggests that the corrosion process usually begins from the pitting sites and then spreads into large areas, and finally damages the steel bar seriously. Based on the visual observation, Beam 1 (40 kN loading) had the largest corrosion areas, and Beam 4 (no loading) had the smallest corrosion areas, suggesting that corrosion areas increased with the increasing load. Therefore, this result indicates that the corrosion of steel bars is related with the loading values. This is in agreement with galvanic current measurements described above. There were no much differences between Beam 2 and Beam 3, suggesting little effects from alternative wetting - drying conditions. This may be resulted from the short test period, and tests in longer terms are needed for further investigations.

(a) Bare steel bars of a beam

(b) Attack on steel bar surface

Fig. 8 Visual observation of corrosion on steel bars

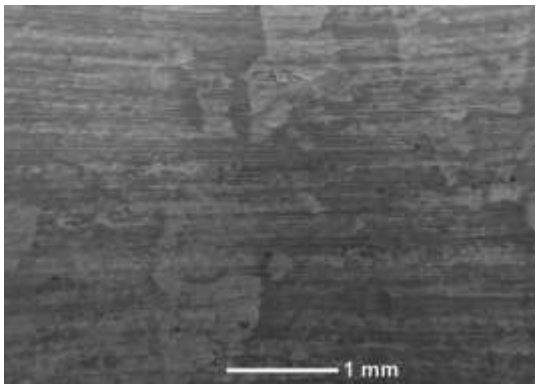

(a) no corrosion

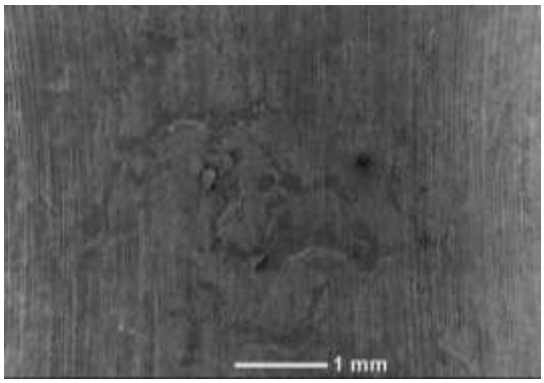

(b) no loading (beam 4)

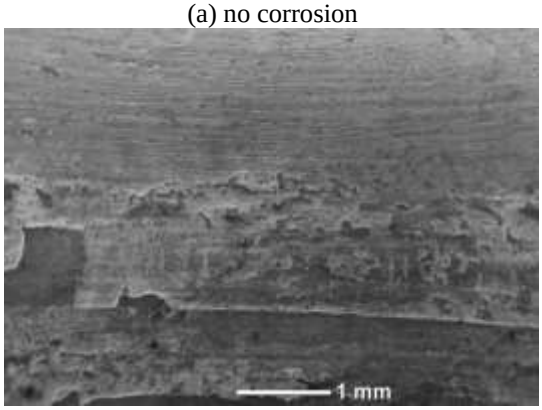

(c) 20 kN loading (beam 2)

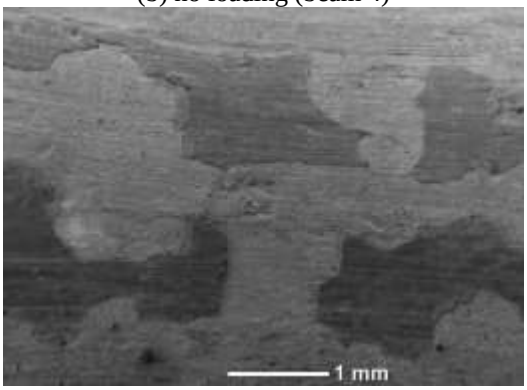

(d) 40 kN loading (beam 1)

Fig. 9 SEM images of corrosion on beams

The SEM images presented in Fig. 9 were used to examine the corrosion of beams subjected to different loads. Fig. 9(a) shows the surface of a steel bar before testing, and the Figs. 9(b)-9(d) show the typical surfaces of steel bars after corrosion testing. It can be seen that only some abrading scratches exist on Fig. 9(a) and that the surface of the sample is smooth. In comparison, it can be observed from Fig. 9(d) that the local surface of specimen was seriously damaged and larger corrosion areas on the surface appeared than the surfaces in Figs. 9(a)-9(c). For instance, the area of the largest pit in beam 1 and beam 4 is roughly 0.6 x 10^{-4} m^2 and 0.24 x 10^{-4} m^2, respectively. There was more apparent corrosion on the surface of Fig. 9(c) than in Fig. 9(b). It confirms again that the larger loads on beams, the deeper and larger corrosion areas occur.

4. Conclusions

This work is a preliminary study on corrosion monitoring of RC structures under simulated marine environmental and loading conditions. Corrosion processes occurring on steel bars under different loads and wetting-drying cycle conditions have been monitored by measuring and comparing galvanic current values. Electrochemical devices were utilised to measure the potential and galvanic currents flowing between different steel bars in each beam, and microscopic methods were applied to observe corrosion patterns. The results indicated that steel corrosion in beams was affected by local stress. The point load could lead to the increase of galvanic currents, and corrosion rates and areas. Pitting corrosion was observed to be the main corrosion form on the surface of the steel bars. It can also be seen that the wetting-drying cycle plays a very limited role in corrosion in this study.

References

Ahmad, S. (2003), "Reinforcement corrosion in concrete structures, its monitoring and service life prediction—a review", *Cement Concrete Comp.*, **25**(4), 459-471.

Alghamdi, S.A. and Ahmad, S. (2014), "Service life prediction of RC structures based on correlation between electrochemical and gravimetric reinforcement corrosion rates", *Cement Concrete Comp.*, **47**, 64-68.

Al Zubaidy, E.A.H. and Al Tamimi, A. (2012), "Reduction of corrosion process in steel bars using inhibitors", *Int. J. Electrochem. Sci.*, **7**, 6472-6488.

Apostolopoulos, C.A. and Papadakis, V.G. (2008), "Consequences of steel corrosion on the ductility properties of reinforcement bar", *Constr. Build. Mater.*, **22**(12), 2316-2324.

Assouli, B., Ballivy, G. and Rivard, P. (2008), "Influence of environmental parameters on application of standard ASTM C876-91: half cell potential measurements", *Corrosion Eng. Sci. Technol.*, **43**(1), 93-96.

Ballim, Y. and Reid, J.C. (2003), "Reinforcement corrosion and deflection of RC beams – an experimental critique of current test methods", *Cement Concrete Comp.*, **25**(6), 25-32.

Berkeley, K.G.C. and Pathmanaban, S. (1990), *Cathodic protection of reinforcement steel in concrete*, Butterworths & Co. Ltd., London, UK.

Cabrera, J.G. (1996), "Deterioration of concrete due to reinforcement steel corrosion", *Cement Concrete Comp.*, **18**(1), 47-59.

Dehwah, H.A.F., Maslehuddin, M. and Austin, S.A. (2002), "Long-term effect of sulfate ions and associated cation type on chloride-induced reinforcement corrosion in Portland cement concretes", *Cement Concrete Comp.*, **24**(1), 17-25.

Díaz, B., Freire, L., Nóvoa, X.R. and Pérez, M.C. (2009), "Electrochemical behaviour of high strength steel

wires in the presence of chlorides", *Electrochimica Acta*, **54**(22), 5190-5198.
Fang, C, Lundgren, K., Plos, M. and Gylltoft, K. (2006), "Bond behaviour of corroded reinforcing steel bars in concrete", *Cement Concrete Res*., **36**, 1931-1938.
Li, G., Yuan, Y.S. and Li, F.M. (2005), "Accelerating effect of wetting-drying cycles on steel bar corrosion in concrete", *J. China Univ. Mining Technol.*, **15**(3), 197-202.
Lomborg, B. (2001), *The skeptical environmentalist: measuring the real state of the world*, Cambridge University Press, Cambridge.
Nwaubani, S.O. and Katsanos, A. (2014), "Effect of alternative de-icers on the corrosion resistance of reinforced concrete bridges and highway structures", *Intechopen*, **24**, 594-614
Ormellese, M., Berra, M., Bolzoni, F. and Pastore, T. (2006), "Corrosion inhibitors for chlorides induced corrosion in reinforced concrete structures", *Cement Concrete Res.*, **36**(3), 536-547.
Pettersson, K. (1998), "Service life of concrete structure including the propagation time", *Concrete under severe conditions 2: environment and loading: Proceedings of the 2nd international conference on concrete under severe conditions*, Troms, Norway.
Poerner, N.W. (2007), *An investigation of variability among residual stress measurement techniques and prediction of machining induced distortion*, Texas Tech University.
Poupard, O., L'hostis, V., Catinaud, S. and Petre-Lazar, I. (2006), "Corrosion damage diagnosis of a reinforced concrete beam after 40 years natural exposure in marine environment", *Cement Concrete Res.*, **36**(3), 504-520.
Pradhan, B. and Bhattacharjee, B. (2009), "Half-cell potential as an indicator of chloride-induced rebar corrosion initiation in RC", *J. Mater. Civil Eng.*, **21**(10), 543-552.
Sakr, K. (2005), "Effect of cement type on the corrosion of reinforcing steel bars exposed to acidic media using electrochemical techniques", *Cement Concrete Res.*, **35**(9), 1820-1826.
Schmitt, G. (2009), "Global needs for knowledge dissemination, research, and development in materials deterioration and corrosion control", *World Corrosion Organization, New York*.
Song, H.W., Ann, K.Y., Pack, S.W. and Lee, C.H. (2010), "Factors influencing chloride transport and chloride threshold level for the prediction of service life of concrete structures", *Int. J. Struct. Eng.*, **1**(1), 131-144.
Tan, Y.J. (2011), "Experimental methods designed for measuring corrosion in highly resistive and inhomogeneous media", *Corrosion Sci.*, **53**, 1145-1155
Torres-Acosta, A.A., Sergio, N.G. and Jorge, T.G. (2007), "Residual flexure capacity of corroded reinforced concrete beams", *Eng. Struct*., **29**(6), 1145-1152.
Wang, H.L., Lu, C.H., Jin, W.L. and Bai, Y. (2011), "Effect of external loads on chloride transport in concrete", *J. Mater. Civil Eng*., **23**(7), 1043-1049.
Wang, Y. and Hao, H. (2012), "Damage identification of steel beams using local and global methods", *Adv. Struct. Eng*., **15**(5), 807-824.
Wang, Y., Zhu, X.Q., Hao, H. and Stewart, M.G. (2008), "Corrosion-induced cracking of reinforced concrete beam: experimental study", *WCEAM-IMS 2008: Engineering asset management-a foundation for sustainable development: Proceedings of the Third World Congress on Engineering Asset Management and Intelligent Maintenance Systems*. Springer-Verlag London.
Yuan, Y., Ji, Y., and Shah, S.P. (2007), "Comparison of two accelerated corrosion techniques for concrete structures", *ACI Struct. J.*, **104**(3), 344-347.

Appendix

Potential and current numerical values recorded from Beams 1, 2, 3 and 4 (Tables 1, 2, 3 and 4).

Table 1 Potential (in V vs. Ag/AgCl reference electrode) and Current (in mA) numerical values of Beam 1

	Potential (in V vs. Ag/AgCl reference electrode)									Current (in mA)							
Day	U1	U2	U3	U4	U5	U6	U7	U8	U9	I1-2	I1-3	I1-4	I1-5	I1-6	I1-7	I1-8	I1-9
1	-0.618	-0.647	-0.624	-0.631	-0.606	-0.627	-0.650	-0.549	-0.634	0.002	-0.047	-0.042	-0.068	-0.016	0.046	-0.195	0.074
2	-0.649	-0.649	-0.633	-0.649	-0.624	-0.643	-0.671	-0.489	-0.649	0.002	0.062	-0.006	0.083	0.004	-0.112	0.431	-0.079
3	-0.651	-0.648	-0.639	-0.653	-0.635	-0.646	-0.665	-0.533	-0.651	0.010	-0.032	0.011	-0.048	-0.014	0.066	-0.025	-0.001
4	-0.661	-0.658	-0.653	-0.672	-0.636	-0.667	-0.674	-0.540	-0.663	0.015	0.040	-0.043	0.108	-0.025	-0.053	0.359	-0.056
5	-0.661	-0.652	-0.658	-0.668	-0.631	-0.666	-0.663	-0.576	-0.660	0.063	0.012	-0.071	0.264	-0.059	-0.031	0.076	0.017
6	-0.676	-0.663	-0.669	-0.678	-0.661	-0.671	-0.669	-0.556	-0.659	-0.048	0.023	0.017	-0.061	-0.052	0.018	-0.180	-0.023
7	-0.677	-0.664	-0.669	-0.675	-0.662	-0.644	-0.663	-0.638	-0.657	0.056	0.024	-0.006	0.057	0.106	0.031	0.114	0.032
8	-0.677	-0.665	-0.669	-0.672	-0.661	-0.666	-0.661	-0.541	-0.656	-0.052	-0.027	0.004	-0.055	-0.030	-0.046	-0.406	-0.007
9	-0.682	-0.668	-0.674	-0.675	-0.664	-0.668	-0.665	-0.555	-0.661	0.022	-0.029	-0.010	0.049	0.033	0.042	0.465	0.024
11	-0.676	-0.665	-0.673	-0.671	-0.666	-0.662	-0.661	-0.578	-0.661	0.036	0.016	0.042	0.030	0.054	0.044	0.185	0.028
12	-0.665	-0.663	-0.669	-0.671	-0.660	-0.665	-0.665	-0.653	-0.661	0.009	-0.018	-0.026	0.022	0.003	-0.006	0.060	0.010
13	-0.662	-0.672	-0.673	-0.672	-0.672	-0.669	-0.668	-0.616	-0.660	-0.030	-0.026	-0.021	-0.015	-0.004	-0.002	0.199	-0.011
14	-0.668	-0.664	-0.669	-0.672	-0.670	-0.663	-0.667	-0.600	-0.663	-0.016	0.008	0.023	0.005	-0.020	-0.003	-0.229	0.014

Table 2 Potential (in V vs. Ag/AgCl reference electrode) and Current (in mA) numerical values of Beam 2

	Potential (in V vs. Ag/AgCl reference electrode)									Current (in mA)							
Day	U1	U2	U3	U4	U5	U6	U7	U8	U9	I1-2	I1-3	I1-4	I1-5	I1-6	I1-7	I1-8	I1-9
1	-0.263	-0.355	-0.152	-0.265	-0.286	-0.267	-0.218	-0.271	-0.153	-0.081	0.084	-0.032	-0.019	0.035	0.115	-0.010	0.103
2	-0.755	-0.783	-0.746	-0.767	-0.743	-0.781	-0.561	-0.757	-0.363	-0.102	0.064	-0.062	0.041	-0.142	0.142	-0.064	0.285
3	-0.309	-0.389	-0.126	-0.333	-0.303	-0.387	-0.318	-0.320	-0.054	-0.179	0.242	-0.100	0.008	0.160	-0.131	0.007	-0.407
4	-0.304	-0.433	-0.247	-0.325	-0.305	-0.332	-0.239	-0.307	-0.251	-0.193	0.267	-0.114	-0.039	-0.126	0.093	0.030	0.082
7	-0.325	-0.454	-0.192	-0.294	-0.302	-0.340	-0.265	-0.309	-0.140	-0.327	0.288	0.034	0.014	-0.157	0.178	0.006	0.090
8	-0.325	-0.463	-0.142	-0.303	-0.304	-0.340	-0.248	-0.312	-0.156	-0.299	0.379	-0.035	0.014	-0.039	0.188	-0.035	0.374
9	-0.331	-0.466	-0.164	-0.306	-0.305	-0.337	-0.207	-0.308	-0.195	-0.302	0.490	-0.029	0.020	-0.025	0.240	-0.020	0.499
10	-0.333	-0.469	-0.160	-0.301	-0.302	-0.334	-0.255	-0.306	-0.149	-0.339	0.578	-0.076	0.069	0.019	0.164	-0.014	0.508
11	-0.339	-0.473	-0.168	-0.304	-0.305	-0.338	-0.218	-0.304	-0.218	-0.337	0.577	-0.031	0.022	-0.029	0.205	-0.007	0.582
14	-0.339	-0.485	-0.169	-0.316	-0.309	-0.342	-0.217	-0.295	-0.190	-0.388	0.614	-0.058	0.024	-0.044	0.440	-0.043	0.573

Table 3 Potential (in V vs. Ag/AgCl reference electrode) and Current (in mA) numerical values of Beam 3

	Potential (in V vs. Ag/AgCl reference electrode)									Current (in mA)							
Day	U1	U2	U3	U4	U5	U6	U7	U8	U9	I1-2	I1-3	I1-4	I1-5	I1-6	I1-7	I1-8	I1-9
1	-0.352	-0.326	-0.350	-0.351	-0.351	-0.351	-0.391	-0.389	-0.326	0.032	-0.036	-0.052	-0.016	-0.015	0.132	-0.170	0.096
2	-0.400	-0.387	-0.414	-0.415	-0.344	-0.415	-0.267	-0.433	-0.363	0.034	-0.039	-0.017	0.080	-0.026	0.187	-0.124	0.060
3	-0.422	-0.398	-0.440	-0.440	-0.413	-0.408	-0.309	-0.428	-0.397	0.079	-0.086	-0.041	0.078	-0.010	0.294	-0.062	0.091
4	-0.435	-0.404	-0.458	-0.458	-0.415	-0.418	-0.305	-0.430	-0.416	0.096	-0.071	-0.081	0.059	0.027	0.175	-0.070	0.037
7	-0.494	-0.427	-0.486	-0.486	-0.431	-0.430	-0.315	-0.472	-0.462	0.128	-0.031	-0.114	0.223	0.135	0.247	-0.003	0.051
8	-0.511	-0.434	-0.493	-0.493	-0.441	-0.465	-0.319	-0.480	-0.470	0.185	0.015	-0.019	0.110	0.139	0.205	0.042	0.056
22	-0.355	-0.301	-0.355	-0.414	-0.363	-0.328	-0.211	-0.316	-0.337	0.076	-0.050	-0.240	0.035	0.140	0.933	0.180	0.061
23	-0.392	-0.354	-0.376	-0.442	-0.376	-0.350	-0.239	-0.350	-0.364	0.080	0.013	-0.138	0.072	0.089	0.281	0.003	0.063
24	-0.408	-0.370	-0.390	-0.463	-0.384	-0.346	-0.249	-0.428	-0.381	0.121	0.017	-0.174	0.137	0.117	0.281	-0.120	0.064
25	-0.387	-0.379	-0.401	-0.474	-0.398	-0.383	-0.258	-0.440	-0.388	0.023	-0.041	-0.272	0.027	0.025	0.337	-0.181	0.015
28	-0.456	-0.407	-0.423	-0.495	-0.416	-0.377	-0.283	-0.467	-0.424	0.171	0.045	-0.155	0.123	0.156	0.306	-0.045	-0.053

Table 4 Potential (in V vs. Ag/AgCl reference electrode) and Current (in mA) numerical values of Beam 4

	Potential (in V vs. Ag/AgCl reference electrode)									Current (in mA)							
Day	U1	U2	U3	U4	U5	U6	U7	U8	U9	I1-2	I1-3	I1-4	I1-5	I1-6	I1-7	I1-8	I1-9
1	-0.580	-0.538	-0.604	-0.529	-0.564	-0.426	-0.596	-0.614	-0.568	-0.038	0.027	-0.055	-0.004	-0.256	0.035	0.052	-0.230
2	-0.591	-0.556	-0.611	-0.554	-0.574	-0.445	-0.605	-0.622	-0.576	-0.097	0.045	-0.063	-0.011	-0.266	0.085	0.152	0.019
3	-0.600	-0.571	-0.614	-0.575	-0.582	-0.457	-0.612	-0.625	-0.589	-0.029	0.014	-0.025	-0.017	-0.143	0.013	0.025	-0.011
4	-0.608	-0.590	-0.618	-0.595	-0.592	-0.486	-0.618	-0.632	-0.601	-0.065	0.019	-0.041	-0.031	-0.307	0.044	0.096	0.048
7	-0.617	-0.619	-0.627	-0.633	-0.619	-0.578	-0.625	-0.641	-0.628	0.023	0.002	-0.032	0.018	0.136	0.003	-0.080	-0.023
8	-0.623	-0.619	-0.579	-0.636	-0.620	-0.583	-0.623	-0.641	-0.628	-0.021	-0.006	0.055	-0.005	-0.134	-0.008	0.075	0.035
9	-0.626	-0.622	-0.629	-0.644	-0.623	-0.587	-0.626	-0.645	-0.630	0.028	0.009	-0.057	0.014	0.135	0.019	-0.073	-0.014
10	-0.622	-0.622	-0.630	-0.644	-0.624	-0.589	-0.625	-0.645	-0.631	-0.025	-0.008	0.069	-0.010	-0.123	-0.020	0.074	0.030
11	-0.624	-0.621	-0.627	-0.619	-0.626	-0.534	-0.623	-0.644	-0.630	0.016	0.004	-0.079	-0.003	0.124	0.002	-0.074	-0.011
14	-0.631	-0.624	-0.632	-0.650	-0.628	-0.594	-0.628	-0.644	-0.630	0.034	0.010	-0.065	0.008	0.115	0.026	-0.056	-0.024
15	-0.633	-0.628	-0.635	-0.632	-0.629	-0.632	-0.632	-0.643	-0.626	0.007	0.001	0.004	0.063	0.010	0.007	-0.045	0.002
16	-0.634	-0.625	-0.637	-0.637	-0.634	-0.629	-0.634	-0.636	-0.634	0.036	-0.007	-0.019	-0.001	0.048	0.011	-0.026	-0.006

17	**-0.616**	**-0.622**	**-0.638**	**-0.650**	**-0.631**	**-0.637**	**-0.636**	**-0.636**	**-0.634**	**0.020**	**-0.039**	**-0.072**	**0.016**	**-0.016**	**-0.002**	**-0.011**	**0.008**
28	**-0.634**	**-0.624**	**-0.644**	**-0.646**	**-0.638**	**-0.632**	**-0.634**	**-0.633**	**-0.631**	**0.038**	**-0.038**	**-0.019**	**-0.009**	**0.019**	**0.004**	**0.009**	**0.004**
29	**-0.634**	**-0.623**	**-0.647**	**-0.654**	**-0.638**	**-0.640**	**-0.635**	**-0.640**	**-0.639**	**0.049**	**-0.066**	**-0.071**	**0.003**	**-0.011**	**0.014**	**-0.015**	**0.004**
30	**-0.635**	**-0.623**	**-0.648**	**-0.655**	**-0.638**	**-0.639**	**-0.634**	**-0.638**	**-0.626**	**0.045**	**-0.049**	**-0.059**	**-0.006**	**0.012**	**-0.003**	**-0.006**	**0.017**
31	**-0.633**	**-0.625**	**-0.650**	**-0.656**	**-0.640**	**-0.641**	**-0.635**	**-0.639**	**-0.633**	**0.030**	**-0.067**	**-0.067**	**-0.014**	**-0.006**	**0.005**	**-0.008**	**0.021**
32	**-0.633**	**-0.624**	**-0.650**	**-0.656**	**-0.640**	**-0.622**	**-0.636**	**-0.646**	**-0.630**	**0.034**	**-0.064**	**-0.063**	**-0.004**	**0.021**	**0.006**	**-0.023**	**0.034**
35	**-0.632**	**-0.623**	**-0.650**	**-0.656**	**-0.641**	**-0.625**	**-0.639**	**-0.647**	**-0.629**	**0.033**	**-0.074**	**-0.067**	**-0.007**	**0.047**	**-0.012**	**-0.031**	**0.032**
36	**-0.632**	**-0.624**	**-0.650**	**-0.656**	**-0.642**	**-0.629**	**-0.639**	**-0.647**	**-0.633**	**0.027**	**-0.071**	**-0.068**	**-0.010**	**0.014**	**-0.006**	**-0.030**	**0.025**
37	**-0.632**	**-0.623**	**-0.649**	**-0.655**	**-0.641**	**-0.642**	**-0.638**	**-0.642**	**-0.631**	**0.089**	**-0.121**	**-0.130**	**-0.050**	**-0.045**	**-0.019**	**-0.044**	**0.030**
38	**-0.632**	**-0.624**	**-0.647**	**-0.654**	**-0.641**	**-0.643**	**-0.639**	**-0.642**	**-0.631**	**0.026**	**-0.059**	**-0.088**	**-0.030**	**-0.032**	**-0.015**	**-0.034**	**0.017**
39	**-0.635**	**-0.624**	**-0.645**	**-0.653**	**-0.642**	**-0.643**	**-0.639**	**-0.643**	**-0.631**	**0.034**	**-0.061**	**-0.070**	**-0.011**	**-0.016**	**-0.002**	**-0.015**	**0.030**
42	**-0.635**	**-0.623**	**-0.646**	**-0.656**	**-0.643**	**-0.639**	**-0.640**	**-0.643**	**-0.631**	**0.032**	**-0.059**	**-0.075**	**-0.014**	**0.006**	**-0.006**	**-0.024**	**0.032**
43	**-0.631**	**-0.622**	**-0.646**	**-0.656**	**-0.642**	**-0.630**	**-0.640**	**-0.647**	**-0.630**	**0.037**	**-0.058**	**-0.076**	**-0.016**	**0.029**	**-0.016**	**-0.043**	**0.029**
44	**-0.630**	**-0.621**	**-0.644**	**-0.654**	**-0.640**	**-0.626**	**-0.638**	**-0.644**	**-0.629**	**0.037**	**-0.065**	**-0.077**	**-0.016**	**0.032**	**-0.017**	**-0.037**	**0.025**
45	**-0.624**	**-0.620**	**-0.645**	**-0.656**	**-0.642**	**-0.626**	**-0.638**	**-0.643**	**-0.632**	**0.032**	**-0.060**	**-0.085**	**-0.018**	**0.033**	**-0.018**	**-0.034**	**0.014**
46	**-0.629**	**-0.620**	**-0.645**	**-0.655**	**-0.641**	**-0.626**	**-0.639**	**-0.643**	**-0.634**	**0.054**	**-0.055**	**-0.079**	**-0.014**	**0.036**	**-0.015**	**-0.029**	**0.015**
49	**-0.626**	**-0.617**	**-0.642**	**-0.653**	**-0.639**	**-0.620**	**-0.637**	**-0.637**	**-0.631**	**0.037**	**-0.070**	**-0.088**	**-0.021**	**0.038**	**-0.033**	**-0.028**	**0.001**
50	**-0.628**	**-0.621**	**-0.646**	**-0.658**	**-0.642**	**-0.623**	**-0.640**	**-0.645**	**-0.635**	**0.027**	**-0.074**	**-0.092**	**-0.020**	**0.044**	**-0.022**	**-0.043**	**0.009**
51	**-0.627**	**-0.620**	**-0.645**	**-0.656**	**-0.641**	**-0.621**	**-0.639**	**-0.644**	**-0.636**	**0.027**	**-0.070**	**-0.087**	**-0.019**	**0.046**	**-0.023**	**-0.041**	**0.002**
52	**-0.628**	**-0.620**	**-0.644**	**-0.656**	**-0.641**	**-0.621**	**-0.640**	**-0.643**	**-0.636**	**0.028**	**-0.071**	**-0.091**	**-0.022**	**0.047**	**-0.030**	**-0.040**	**-0.003**
53	**-0.629**	**-0.622**	**-0.646**	**-0.659**	**-0.643**	**-0.623**	**-0.643**	**-0.649**	**-0.639**	**0.028**	**-0.072**	**-0.093**	**-0.022**	**0.030**	**-0.028**	**-0.041**	**-0.004**
56	**-0.625**	**-0.622**	**-0.643**	**-0.656**	**-0.642**	**-0.621**	**-0.642**	**-0.645**	**-0.638**	**0.017**	**-0.067**	**-0.089**	**-0.025**	**0.044**	**-0.036**	**-0.044**	**-0.007**